Research Article

Received: 6 January 2021 Revised: 23 February 2021 Accepted article published: 26 March 2021 Published online in Wiley Online Library:

(wileyonlinelibrary.com) DOI 10.1002/pi.6226

High-performance and cost-effective melt blended poly(ether ether ketone)/expanded graphite composites for mass production of antistatic materials

Mozaffar Mokhtari,[a]* Edward Archer,[a] Noel Bloomfield,[b] Eileen Harkin-Jones[a] and Alistair McIlhagger[a]

Abstract

In this study unfunctionalized expanded graphite (EG) was incorporated into poly(ether ether ketone) (PEEK) using twin-screw extrusion and injection moulding to manufacture cost-effective PEEK/EG composites for mass production of high-performance antistatic materials. Direct current electrical conductivity, morphology, rheological and thermal properties of the composites were investigated. At an EG loading of 5 vol%, the electrical conductivity exhibited an abrupt increase to 1.45×10^{-5} S m^{-1} which was in the required range of electrical conductivity of antistatic materials. The frequency dependence of the storage modulus of the melt containing 2 vol% EG decreased significantly at low frequencies. Viscosity did not increase much with the addition of EG in comparison with other nanofillers such as carbon nanotubes. The crystallinity of PEEK increased to 41.11% from 35.87% upon addition of 3 vol% EG. EG improved the thermal stability of PEEK by an increase in the initiation temperature of its decomposition steps.

Keywords: PEEK; high-performance; cost-effective; expanded graphite; antistatic

INTRODUCTION

Electrostatic discharge (ESD) protection is an important requirement for applications of polymeric materials in industries such as automotive, aeronautics and aerospace. For example, due to the electrical insulation properties of polymeric materials used in satellites, low-energy electrons accumulate on their surfaces which causes an increase in the surface electric potential and electrostatic discharge phenomena which is at the origin of many spacecraft failures.[1,2] The electrical conductivity of polymers must be greater than 10^{-6} S m^{-1} to avoid the build-up of static charge.[3] The most common strategy to enhance the electrical conductivity of polymeric materials is incorporation of carbon based electrically conductive fillers such as carbon nanotubes (CNTs) and graphite.[4–6] Expanded graphite (EG) is obtained by a rapid thermal expansion of graphite flakes. It keeps a sheet-like structure but with a large interlayer spacing and contains plentiful multipores ranging from 2 nm to 10 μm. EG combines the lower price and the layered structure of clays with the superior thermal and electrical properties of CNTs, thus making it a promising substitution for both clay and CNTs to manufacture cost-effective multifunctional nanocomposites.[7–12]

Low volume fractions of EG were applied successfully to enhance the electrical conductivity of polymers such as poly(methyl methacrylate),[13] polysulfide, polystyrenes,[14,15] poly (styrene-*co*-acrylonitrile),[16] poly(4,4′-oxybis(benzene) disulfide)[17] and nylon-6[18] to the semiconducting and conducting regions. Solution mixing[7,13] and *in situ* polymerization[14–18] were exploited to prepare the above-mentioned polymer/EG nanocomposites. Shen *et al.*[19] compared the effect of solution and melt mixings on the electrical conductivity values of maleic anhydride grafted polypropylene/EG nanocomposites and demonstrated that the electrical conductivity percolation threshold of the melt blended nanocomposites was higher. In solution mixing and *in situ* polymerization the polymer viscosity is lower and polymer chains penetrate more into the interlayer spaces of the EG platelets, increase their distances and enhance EG dispersion. Also, the shear level in these processing methods is less and the aspect ratio of the filler does not reduce significantly during the processing, thus leading to an electrical percolation threshold at lower EG volume fractions. On the other hand, in melt mixing high shear stress is applied to overcome van der Waals interactions of the EG platelets, reduce the agglomerate size and improve the EG dispersion

* *Correspondence to: M Mokhtari, School of Engineering, Ulster University, Newtownabbey, UK. E-mail: m.mokhtari@ulster.ac.uk*

a *School of Engineering, Ulster University, Newtownabbey, UK*

b *Denroy Plastics, Bangor, UK*

state. This reduces the EG aspect ratio and the electrical percolation threshold is increased.[20,21] Nevertheless, melt mixing is the method of choice in commercial polymer processing and it is critical to assess this pathway if new electrically conductive composite materials are to be successful.[22,23]

The unique properties of PEEK such as high temperature resistance, excellent mechanical performance and chemical resistance, outstanding dimensional stability and biocompatibility have generated a lot of interest in PEEK as a substitution for metals in industries such as biomaterials and aerospace.[24–30] However, PEEK has low electrical conductivity which limits its applicability as a high performance ESD material.[31–36] To enhance its electrical conductivity, carbon fillers such as graphene nanoplatelets (GNPs) and CNTs have been added to PEEK through solution mixing and melt blending.[31,37–41] Díez-Pascual *et al.*[37] and Bangarusampath *et al.*[39] reported a sharp increase in room temperature volume electrical conductivity of PEEK to about 10^{-3} S cm^{-1} with the incorporation of 0.1 wt% single-walled CNTs using stirring and ultrasonication and 1–1.5 wt% multi-walled CNTs via melt blending, respectively. Mohiuddin and Hoa[35] showed that the electrical conductivity of melt blended PEEK/multi-walled CNT composites increased sharply at about 3.5 wt % loading of multi-walled CNTs indicating that the electrical percolation threshold had occurred. Chen *et al.*[42] reported that PEEK/GNP composites prepared by the wet and dry methods showed electrical percolation thresholds between 1 and 5 wt% and electrical conductivity values of 4.54×10^{-3} S cm^{-1} and 4.35×10^{-3} S cm^{-1}, respectively. The electrical percolation threshold of PEEK/GNP composites manufactured by Pan *et al.*[41] happened at 3 wt% with an electrical conductivity of 10^{-5} S cm^{-1}.

Compared with CNTs and GNPs, EG is a more cost-effective, electrically conductive filler that has been widely incorporated into other thermoplastics. However, only one study has been identified for electrically conductive PEEK/EG nanocomposites and this used solution processing to manufacture the composite. This achieved a promising electrical percolation threshold of about 10^{-1} S cm^{-1} at 1.5 wt% EG loading and conductivities of 3.24 S cm^{-1} and 12.3 S cm^{-1} for 5 and 10 wt% EG loaded composites respectively.[34] Solution processing is not a particularly important technique in commercial polymer processing, so it is of interest to examine the processability and performance of PEEK/EG composites via commercially relevant melt blending. To the best of our knowledge, studies of the electrical properties of melt blended PEEK/EG composites have not yet been published.

In this study, EG without any surface chemistry modification was used to manufacture PEEK/EG composites. The composites were prepared via twin-screw extrusion followed by injection moulding. The effect of the loading of EG on the morphological, rheological, thermal and electrical properties of PEEK was investigated. The dispersion state of EG was examined via SEM and melt rheology. Crystallinity and melting behaviour and thermal stability of the samples were characterized by DSC and TGA respectively.

EXPERIMENTAL

Materials

A medium viscosity grade of PEEK (VESTAKEEP 2000P) with a melt volume flow rate (380 °C/5 kg) of 70 cm^3 (10 min)$^{-1}$ was purchased from Evonik (Marl, Germany). EG powder (GFG130) with a mean diameter of 130 μm was kindly provided by SGL Carbon (Wiesbaden, Germany) . The EG density is assumed as the graphite theoretical density of 2.28 g cm^{-3} and the PEEK density is 1.3 g cm^{-3}.[43]

Preparation of composites

The PEEK and EG powders were dried in an oven at 170 °C for 12 h before use and premixed at various compositions. A co-rotating twin-screw extruder (Rheomex PTW16/40 OS) with diameter of 16 mm and $L/D = 40$ was used to compound the PEEK and EG into pellets. It was operated at a screw speed of 45 rpm with heating zone temperatures as shown in Fig. 1. The exact temperature of the melt in the extruder was 370 °C which was measured in zone 9. The in-house screw configuration shown in Fig. 1 was utilized to improve the EG powder distribution and dispersion in PEEK. The screw elements were composed of feed screw elements for the forward and reverse conveying of materials in the feeding, conveying, reverse, venting and extrusion sections of the extruder and mixing elements of 90° and 0° for providing 30°, 60° and 90° twist angles for the melting and mixing sections of the extruder. The compositions of the prepared compounds are shown in Table 1.

An injection moulder (SmartPower 35/130 UNILOG B8) was used to mould the compounded pellets into dumbbells with overall length, overall width, thickness and gauge length of 170, 10, 4 and 8 mm respectively for subsequent testing and characterization. The composite pellets were dried in an oven at 100 °C overnight before the injection. The heating zone temperatures, injection and holding pressures, cooling time and mould temperature of the injection moulding were 320/380/385/390 °C, 2000 bar, 1200 bar, 60 s and 220 °C, respectively.

Material characterization

SEM

SEM (Hitachi SU5000) was used to investigate the distribution and dispersion of the EG platelets in PEEK. The fracture surface of the samples was achieved by a rapid cryogenic fracture. A thin layer of

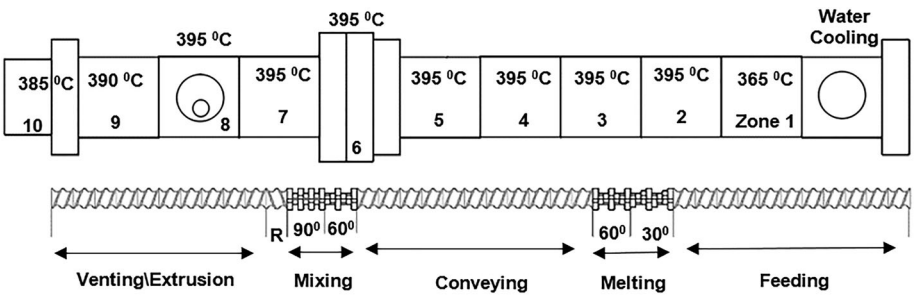

Figure 1. The schematic picture of the processing conditions of the twin-screw extruder.

gold was coated on the fractured surface of the samples with a sputter coater to minimize the charging effect.

DSC

DSC tests were carried out (TA Q100) to study the thermal transitions of the composites. DSC specimens were cut from the extruded pellets. 8 mg of each sample was sealed in standard aluminium hermetic pans. Every test included four cycles under a nitrogen flow rate of 50 mL min^{-1}. In the first and second heating cycles the specimen was heated to 390 °C at a rate of 10 °C min^{-1} and held isothermally for 10 min to remove thermal and stress histories. Then the specimen was cooled to 40 °C and heated up to 390 °C again at the same rate. The melt temperature (T_m) was determined from the melting peak of the last heating cycle. The crystallization temperature T_c and its onset (T_{co}) and endset (T_{ce}) were obtained from the maximum, onset and endset of the crystallization peak of the cooling cycle. The ratio of the melting enthalpy ΔH_m (corrected for the amount of PEEK) from the fourth cycle and the enthalpy of fusion of ideal PEEK crystal ($\Delta H_f = 130$ J g^{-1}) was applied to estimate the degree of crystallinity of PEEK in the composites (X_c).[44] The overall crystallization time was obtained using

$$t_c = \frac{T_{co} - T_{ce}}{a} \quad (1)$$

where a is the cooling rate. Each test was done three times.

TGA

TGA tests were conducted (TA Q600) in an air medium. For study of the degradation mechanism and thermal stability of the composites, TGA specimens were cut from the extruded pellets. The mass of a specimen was 10 mg. Every test specimen was heated to a temperature of 1000 °C at a heating rate of 10 °C min^{-1}. Every test was done three times.

Rheology

The rheological properties of the melt were measured using a rheometer (AR 2000) with 25 mm steel parallel plates at a gap setting of 1 mm. The measurements were carried out by the flow and oscillation methods at 370 °C (the exact melt temperature in the extruder) as a function of shear rate and angular frequency. Frequency and shear rate were changed between 0.06 and 600 rad s^{-1} and 0.001 and 10 s^{-1} respectively. A strain amplitude of 6.25×10^{-3}, which is within the linear viscoelastic region, was chosen for the oscillation test.

Electrical conductivity (EC)

The volume resistivity of low conductivity PEEK composites was measured with an electrometer/high resistance meter (Keithley 6517B) and the volume resistivity of moderately conductive composites (resistance below 10^6 Ω) was measured using an interactive digital source meter (Keithley 2450) at a temperature of 18 °C and humidity of 75%. The samples were cut from the same shoulder of the dumbbell to a size of $18 \times 18 \times 1.5$ mm^3. They were placed between two electrodes and a potential difference was applied between them. Both surfaces of the samples were coated with silver paste to reduce the contact resistance between samples and electrodes. The resistance (R) was obtained directly

Table 1. Details of the composites

PEEK/GFG130	EG vol%	EG wt%
PEEK	0	0
0.5%	0.5	0.9
1%	1	1.7
2%	2	3.5
3%	3	5.2
5%	5	8.5
7%	7	11.7

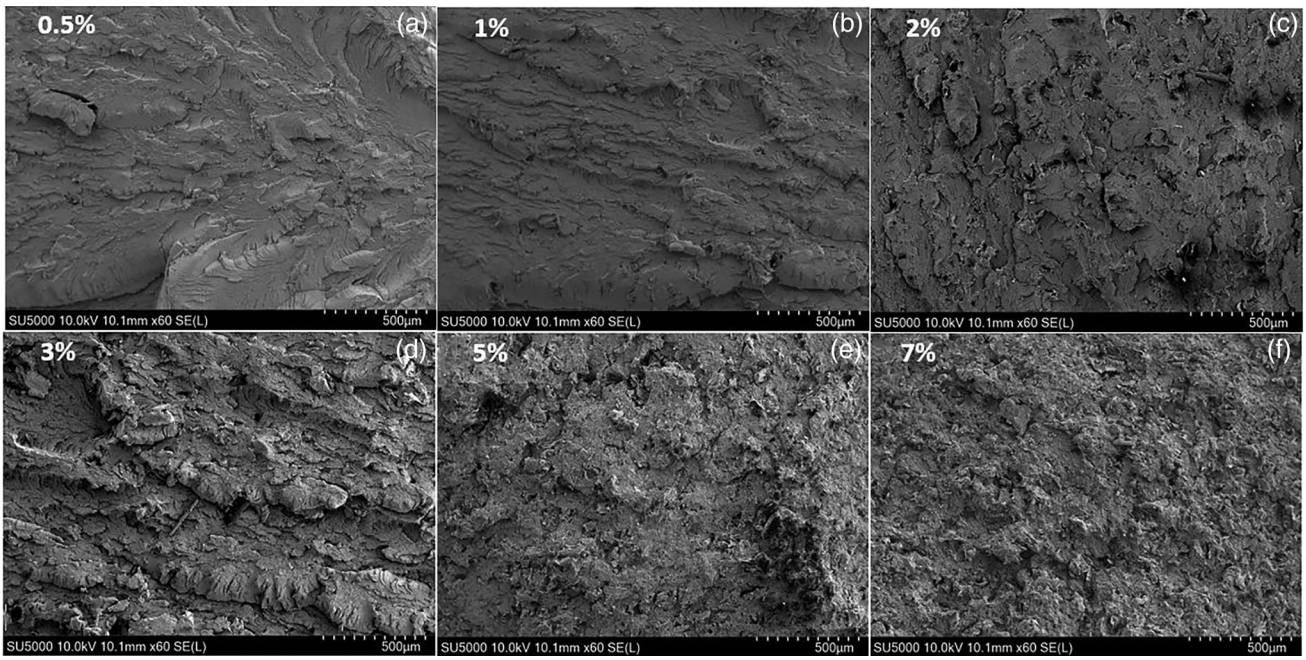

Figure 2. SEM images of PEEK/EG composites at low magnification.

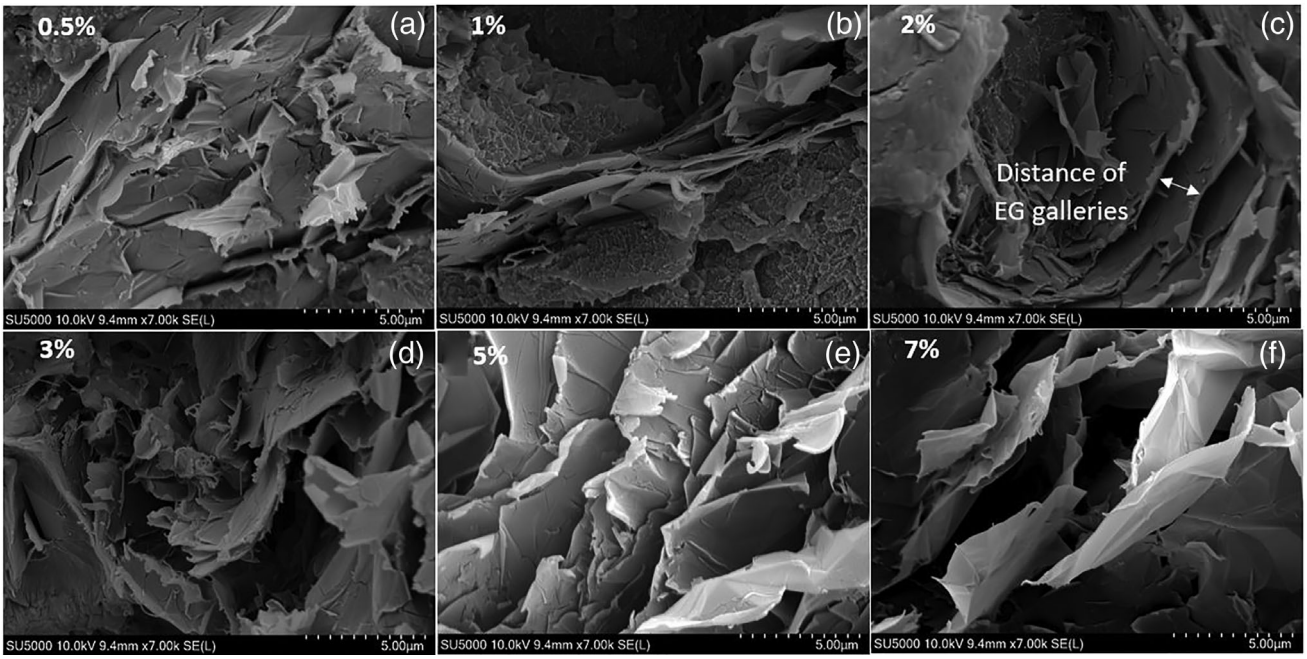

Figure 3. SEM images of the PEEK/EG composites at high magnification.

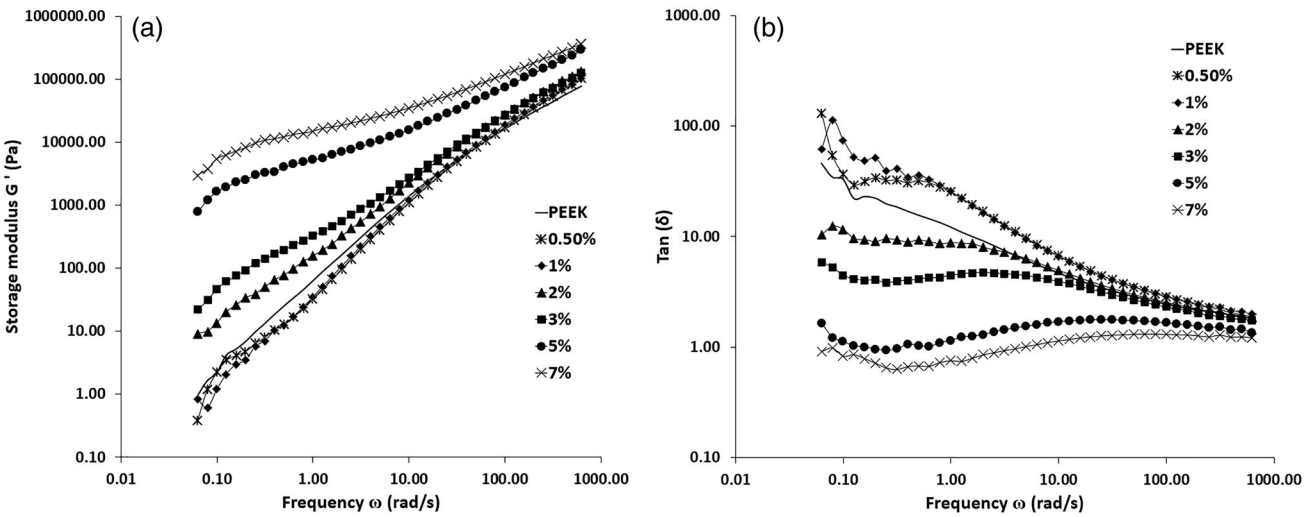

Figure 4. Storage modulus (a) and tan δ (b) of the PEEK/EG composite melts *versus* angular frequency for different EG loadings at 370 °C.

from the instruments and volume resistivity (ρ) was calculated using

$$\rho = RA/L \quad (2)$$

L is the sample thickness and A is the cross-sectional area of the sample. The electrical conductivity is the reciprocal of the volume resistivity.

RESULTS AND DISCUSSION

Morphology analysis

To evaluate the dispersion of EG in the PEEK matrix, SEM images were taken from the fracture surfaces of the injection moulded samples. SEM images of the PEEK/EG composites at two different magnifications are shown in Figs 2 and 3.

A sudden evaporation of intercalate in the expansion process of EG causes a 100 times expansion in the thickness direction of the graphite crystal which results in a huge increase in its volume. After the expansion, EG forms a loose and porous network structure that consists of a lot of tangled sheets with thickness and diameter on the nanometre and micrometre scale respectively. The structure obtained has a high surface area and graphite nanosheets with a thickness less than 100 nm.[20,45,46] Additionally, the large pores and large surface area ease processing of EG loaded polymers, and functional groups such as –OH and –COOH, resulting from the expansion, on the surfaces and the pores of EG galleries can affect the adsorption of polymer molecules onto the pores.[13]

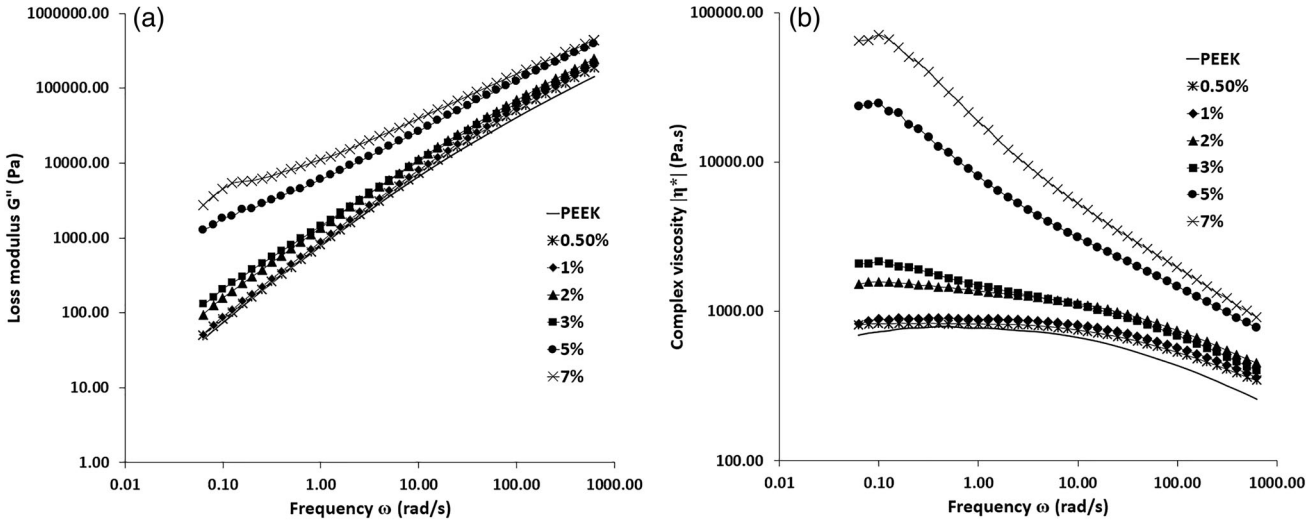

Figure 5. Loss modulus (a) and complex viscosity (b) of the PEEK/EG composite melts *versus* angular frequency for different EG loadings at 370 °C.

Further exfoliation of EG galleries is achieved via the shear stress applied during processing and penetration of the polymer molecules into the gallery spaces. The dispersion level of EG in the PEEK matrix and interfacial morphology can be seen in Figs 2 and 3. They indicate that, with increasing EG content, the dispersion quality increases and the EG galleries are exfoliated more. In addition, the intercalation of PEEK chains into the EG pores supports the EG platelets internally preventing collapse and maintaining their network structure, which is helpful in building a three-dimensional filler network for enhancing electrical conductivity.[19,20,47]

Rheological properties of PEEK/EG composites

Linear viscoelastic properties

The linear viscoelastic properties of the PEEK/EG composite melts as a function of EG loading were studied at a temperature of 370 °C to estimate the dispersion level of EG in the composites. As shown in Fig. 4(a) the frequency sweep graphs of the composites indicate different behaviour depending on the EG concentration. The neat PEEK chains were fully relaxed and exhibited standard polymer viscoelastic behaviour. Here the linear viscoelastic spectrum of the storage modulus (G') exhibits three characteristic regions separated by the lowest relaxation time (τ_0) and the longest relaxation time (reptation time τ_N) of the polymer chains. In the high frequency region $w > \tau_0^{-1}$, the dependence of storage modulus on frequency becomes very weak due to the lack of relaxation processes at such a time scale; at intermediate frequencies $\tau_N^{-1} < w < \tau_0^{-1}$, $G'(w) \sim w^{0.5}$ and segmental motions of the polymer chains or Rouse relaxation processes occur; and at low frequencies $w < \tau_N^{-1}$, $G'(w) \sim w^2$ and terminal relaxation processes (reptation or long-range molecular motions) occur. Generally, particle inclusion increases the magnitude of the storage modulus of composites at all frequencies.

As shown in Figs 2(a) and 2(b) there were not enough particle contacts in the samples containing 0.5 and 1 vol% to form a three-dimensional network of the EG galleries. Hence, it is clear from Fig. 4(a) that the storage modulus spectrum of these composites is not affected. However, the 0.5% and 1% samples have an unexpected decrease in G' compared with the neat PEEK at low and intermediate frequencies. It is obvious from Figs 2(a) and 2 (b) that, at these loadings, EG spheres of rotation did not intersect and there was plenty of space to slip over each other due to the applied shear. The friction coefficient of EG platelets is lower than that of neat PEEK allowing slipping and orientation of the polymer chains, reducing entanglements and leading to an increase in Rouse and terminal relaxation processes.[48] Hence, the decrease in Rouse and reptation relaxation times of the polymer chains leads to a reduction in G' of the mentioned samples at low and intermediate frequencies. Also, as shown in Fig. 4(b), the increase in tan δ values at the low EG loadings of 0.5 and 1 vol% compared with neat PEEK confirm the reduction in elasticity of the composites. However, it is clear from Figs 5(a) and 5(b) that, unlike G' and tan δ, there are small increases in the values of G'' and the complex viscosity of the low EG content composites due to the flowability restriction created by the EG platelets.

The storage modulus as a function of EG volume fraction, at a fixed frequency of 0.1 rad s^{-1}, is plotted in Fig. 6 and shows a rapid increase in the storage modulus of the composite melt at 2 vol% of EG.[49] Also, it can be seen in Fig. 4(a) that the storage modulus of the composite containing 2 vol% of EG presents a significant deviation from the standard terminal behaviour at low frequencies and there is a reduction in the dependence on angular frequency indicating attainment of rheological percolation. It is obvious from Fig. 2(e) that filler–filler interactions increased and a three-dimensional EG network was formed.[50–52] The possible elastic filler–filler interactions and the immobilization of the polymer segments near the particles at the interphase regions result in significant enhancements in elasticity and an increase in the reptation time of the PEEK chains. In the low frequency region, the characteristic relaxation time is the reptation time of the PEEK/EG composites and the characteristic time of the deformation process is the inverse of the angular frequency of the small amplitude oscillation test. With an abrupt increase in the reptation time at the rheological percolation threshold, the Deborah number increases and the liquid-like behaviour of the composite melt changes to solid-like behaviour; the time-independent or elastic portion of the composite melt increases sufficiently that the storage modulus is independent of the angular frequency.[52–56] Also, it is obvious from Fig. 4 (b) that tan δ decreased with increase in the EG concentration at the rheological percolation threshold, showed a swift decrease and at low frequency ranges was almost independent of frequency.[57]

Polymer International published by John Wiley & Sons Ltd on behalf of Society of Industrial Chemistry.

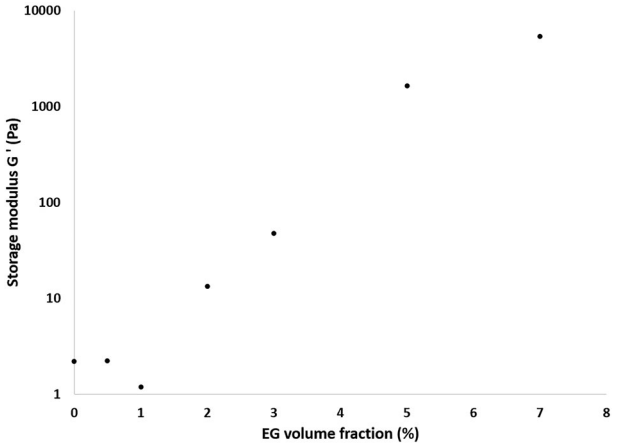

Figure 6. Storage modulus as a function of the EG volume fraction at a fixed frequency of 0.1 rad s^{-1}.

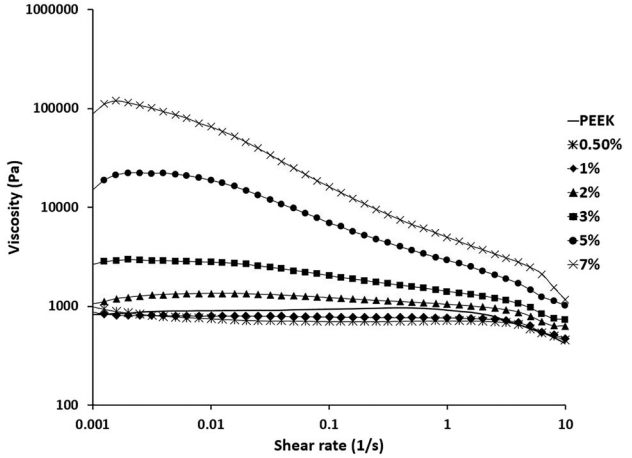

Figure 7. Steady shear viscosity of PEEK/EG composite melts *versus* shear rate for different EG loadings at 370 °C.

Figure 5(b) indicates the complex viscosity of the composites at different EG loadings. Viscosity increases with EG loading especially at low frequencies which is related to the increase in particle–polymer interactions and the reduction in flowability of the PEEK chains. Also, an abrupt increase in viscosity and a change of viscosity behaviour from Newtonian to shear thinning at lower frequencies is observed at the rheological percolation threshold. It can be seen from Fig. 4(b) that the values of tan δ at and after the rheological percolation threshold are close, equal and lower than 1 which means that the energy dissipation capability of the composite melt is reduced notably due to the formation of a semi-solid and elastic EG network. The kinetic energy at low frequencies could not be dissipated by chain motions leading to the breakage of elastic van der Waals filler–filler interactions, the orientation of the platelets in the flow direction and shear thinning behaviour at and after the rheological percolation threshold.

Steady shear behaviour

The steady shear behaviour of the PEEK/EG composites as a function of EG loading was studied at 370 °C to estimate the processability of the composites. Figure 7 shows the dependence of the shear viscosity of the PEEK/EG composites on shear rate. The zero-shear viscosity of the composites with EG loadings well above the rheological percolation threshold was increased and an earlier onset of shear thinning behaviour at low shear rates was observed.[58,59] An increase in zero-shear viscosity and a shear thinning behaviour at long times or low shear rates are indicative of a percolated filler network and strong filler–filler interactions. On the other hand, due to the orientation of the EG platelets in the flow direction at high shear rates, the EG platelets had a relatively small influence on the values of shear viscosity and the composites also displayed a strong shear thinning behaviour at high shear rates. These EG platelets cause a non-Newtonian response at all shear rates at and beyond the rheological percolation threshold.[60,61] The comparison of complex viscosity and shear viscosity in Figs 5(b) and 6 shows that the empirical Cox–Merz rule, $\eta^*(w)=\eta(\dot{\gamma})$ for $w=\dot{\gamma}$, failed for the composites, especially for those with EG loadings well above the rheological percolation threshold. The values of complex viscosity are higher than the values of shear viscosity especially at the lower shear rates which suggests some orientation and alignment of the EG platelets in the steady shear test even at low shear rates.[59]

In addition, the value of viscosity at and beyond the rheological percolation threshold does not increase much compared with the viscosity of the neat PEEK at the higher shear rates more typical of polymer processing which is positive for processing of these materials. Papageorgiou *et al.*[62] also found that the incorporation of 5 and 10 wt% of GNP into PEEK did not significantly increase the viscosity of neat PEEK. It is important to point out that Bangarusampath *et al.*[39] reported a significantly higher viscosity of PEEK filled with CNTs at the same filler content, making the processing of the nanocomposites very challenging. A higher melt viscosity not only needs more energy and higher temperatures for processing but also increases the shear stress level in the extruder die which can lead to melt fracture and thermal decomposition of the PEEK. Therefore, since EG does not significantly increase PEEK viscosity at typical processing shear rates it has an advantage compared with other conductive nanofillers in enhancing the electrical conductivity of PEEK.

DSC

The effect of EG loadings on glass transition temperature, crystallization and melting behaviours of the composites was evaluated by DSC under a non-isothermal condition. The results are shown in Table 2 and Fig. 8. It is clear from Table 2 that incorporation of EG into PEEK does not significantly affect the glass transition temperature of the composites.[63]

Adding fillers to a polymer matrix can affect its crystallization behaviour through a nucleation effect and by altering the mobility of the polymer chain segments via a confinement effect. If the chain mobility confinement effect is dominant during the crystallization process, the crystallization temperature shifts to lower values and the degree of crystallinity decreases. Otherwise, they increase due to occurrence of heterogeneous crystallization. In heterogeneous crystallization, fillers act as nucleation agents that reduce the nucleation barrier energy for crystallization.[64,65] As presented in Table 2 and Fig. 8(b), the onset and peak of the crystallization temperature increased remarkably at low EG loadings due to the nucleation effect of the EG platelets. Higher values of T_c lead to fewer defects in the PEEK crystals and higher melt temperatures in the composites.[66] Pan *et al.*[41] manufactured PEEK/GNP nanocomposites via the combination of a ball mill and a hot press. They found that the onset and peak of crystallization temperature and crystallinity degree of the nanocomposites

Table 2. Non-isothermal crystallization parameters of PEEK/EG composites obtained from the DSC measurements

EG content (vol%)	T_g (°C)	T_m (°C)	ΔH_m (J g^{-1})	X_c (%)	T_c (°C)	T_{co} (°C)	T_{ce} (°C)	t_c (min)
0	150	342	50.15	35.87	292	297	285	1.2
0.5	150	343	52.77	40.59	298	302	292	1.0
1	149	343	52.38	40.29	299	303	295	0.9
2	149	343	53.37	41.05	301	305	296	0.9
3	149	343	53.44	41.11	301	305	296	0.9
5	148	344	49.91	38.39	303	307	298	1.0
7	149	344	49.88	38.37	303	307	298	1.0

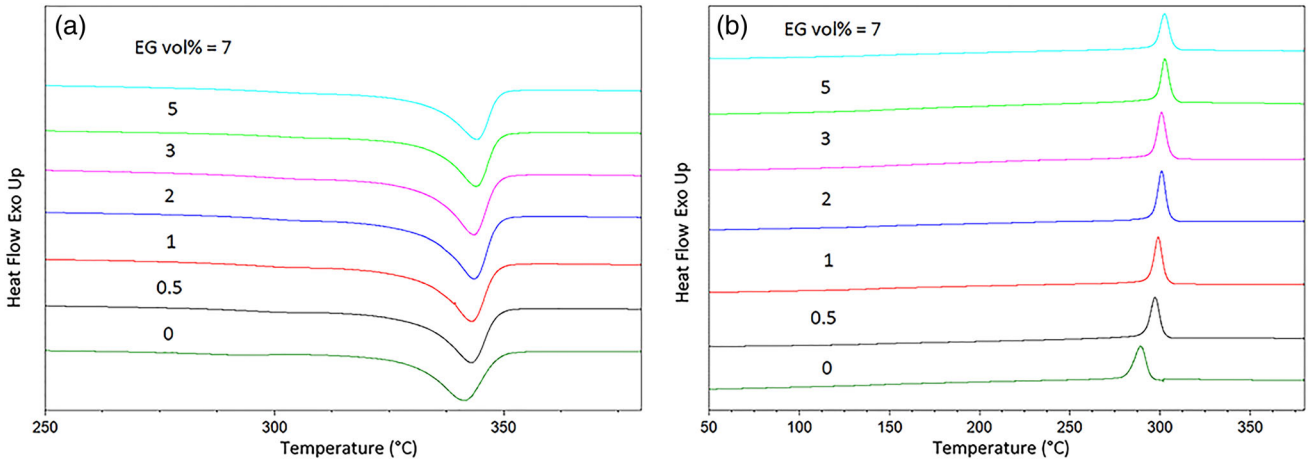

Figure 8. DSC results of the PEEK and composite samples at 10 °C min^{-1}: (a) second heating scan; (b) cooling scan.

increased up to a GNP loading of 5 wt% due to the nucleation promotion. The values of these properties reduced at higher GNP contents due to reduction of polymer chain mobility. In another study, Díez-Pascual *et al*. incorporated CNTs into PEEK through a combination of solution mixing and melt blending. The CNTs decreased the temperature of crystallization of the nanocomposites due to confinement and reduction of PEEK chain movement.[67]

It is clear from Fig. 8(a) and Table 2 that the crystallinity degrees of the composites are higher than that of neat PEEK due to heterogeneous crystallization. The crystallinity degree increases up to 3 vol% of EG and then drops due to a reduction of chain mobility.[68]

Yu *et al*.[69] prepared PEEK/graphene nanocomposites using the combination of a ball mill, melt blending and solution mixing. They found that the degree and temperature of crystallization of the nanocomposites decreased compared with neat PEEK because of the reduction of polymer mobility. In another study, Alvaredo *et al*.[70] utilized melt blending to add GNPs to a PEEK matrix. The GNP loading increased the temperature of crystallization of the nanocomposites with no change in the degree of crystallinity compared with neat PEEK.

Crystallization rate is a crucial parameter in the processing of thermoplastics. The introduction of EG to the PEEK matrix decreases the overall crystallization time and will therefore reduce cooling cycle times. PEEK is a semicrystalline polymer and its ultimate mechanical properties are strongly dependent on its crystallization behaviour; therefore, simultaneous increase of PEEK crystallization rate and degree by adding EG can be very promising in tailoring its properties during processing and annealing.[71,72] Chen *et al*.[42] discovered that increasing the loading of GNP flakes from 0.1 to 10 wt% in PEEK slowed the crystallization rate although it increased X_c. Yu *et al*.[69] found that the overall crystallization time of PEEK/graphene nanocomposites increased with increase in graphene content, but it was always lower than that of neat PEEK.

TGA

As shown in Fig. 9 the thermal decomposition of neat PEEK and the composites in air exhibits a two-step decomposition. In the first step about 30% mass loss occurs within a 50 °C window due to chain scission of ether and ketone bonds. The remaining polymer mass at the end of this step was carbonaceous char. In the second decomposition step, the carbonaceous char obtained from the first step is oxidized.[73–75] The first and second decomposition steps of virgin PEEK started at 546 and 595 °C respectively and inclusion of 0.5 and 7 vol% of EG increased these temperatures to 556 and 606 °C and 562 and 613 °C respectively which meant that EG enhanced the thermal stability of PEEK. The enhancement can be attributed to limitation of the thermal movements of the PEEK chains close to the EG surfaces and the confinement of the decomposition products due to the gas barrier properties of the layers of EG.[36]

Electrical conductivity

The electrical conductivity of polymer composites is influenced significantly by the dispersion state of the fillers which is determined by alignment, concentration and properties of the fillers and the filler–filler and filler–matrix interactions.[37,76] The effect

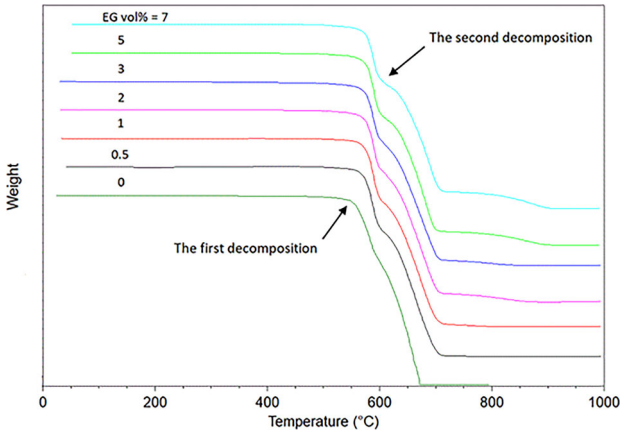

Figure 9. TGA results of the PEEK and composite samples in air medium at a heating rate of 10 °C min^{-1}.

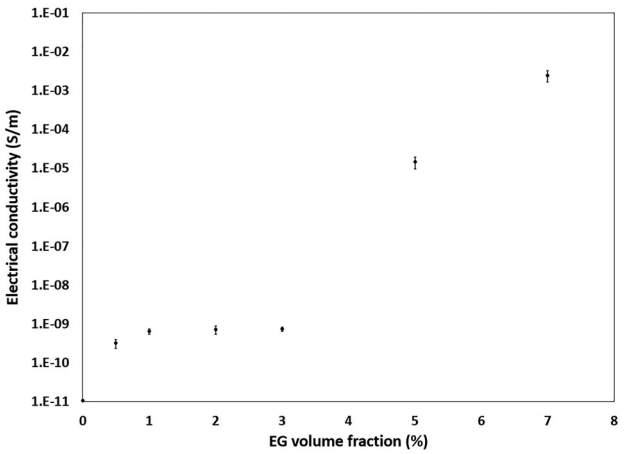

Figure 10. DC volume electrical conductivity of the PEEK/EG composites at room temperature.

of EG loading on the electrical conductivity values of the PEEK/EG composites at room temperature was analysed, and the result is shown in Fig. 10. Like most polymers, PEEK is an electrical insulator and the addition of a conductive filler like EG will impart conductivity if a conductive filler network can be formed. At low EG content, the electrical conductivity values of the composites increase only slightly because, as shown in Figs 2(a)–2(d), the EG platelets are isolated from each other and the conductance of the composites is governed mostly by the conductivity value of the insulated PEEK.[77,78] An abrupt rise in the electrical conductivity of the composites occurs at an EG content of 5 vol% suggesting that a three-dimensional filler network has been formed and a transition from insulator to semiconductor has occurred. The porous structure of the EG fillers is very effective in promotion of conductive networks.[79] As shown in Fig. 3(e), at the percolation threshold, PEEK molecules penetrated into gallery spaces of EG platelets causing further delamination.[10,13,21,80,81] It is precious to mention that the rheological percolation threshold is significantly smaller that the electrical one. The difference can be ascribed to a shorter required particle-particle distance for electron tunnelling as the predominant mechanism of electrical conductivity as compared with that required for the confinement of polymer chains motions at the rheological percolation threshold.[57] With an increase of EG content beyond the electrical percolation threshold, the electrical conductivity increases gently since more particles are available to contact and form conductive paths.[80,82] The electrical conductivity values of composites containing 5 and 7 vol% of EG are 1.45×10^{-5} and 2.40×10^{-3} S m^{-1} which are higher than required electrical conductivity for antistatic applications.[3] However, Goyal obtained much higher values of electrical conductivity for PEEK/EG composites than this research due to the better dispersion quality of EG platelets in the PEEK matrix achieved by using an ultrasonic tip in solution mixing.[34]

CONCLUSIONS

PEEK/EG composites were manufactured via twin-screw extrusion and subsequent injection moulding. EG platelets promoted nucleation and increased the PEEK crystallinity significantly and enhanced its thermal stability. The rheological and electrical percolation thresholds occurred at EG loadings of 2 and 5 vol% respectively. The viscosity of the composite did not increase much at the electrical percolation threshold suggesting that the material will be suitable for melt processing and mass production. The electrical conductivity value at the electrical percolation threshold was in the required range of electrical conductivity of ESD materials.

ACKNOWLEDGEMENTS

The North West Centre for Advanced Manufacturing (NW CAM) project is supported by the European Union's INTERREG VA Programme, managed by the Special EU Programmes Body (SEUPB). The views and opinions in this document do not necessarily reflect those of the European Commission or the Special EU Programmes Body (SEUPB). If you would like further information about NW CAM please contact the lead partner, Catalyst, for details.

REFERENCES

1 Rival G, Paulmier T and Dantras E, *Polym Degrad Stab* **168**:108943 (2019).
2 Leach RD and Alexander MB, *Failures and Anomalies Attributed to Spacecraft Charging*. NASA, Huntsville, AL (1995).
3 Díez-Pascual AM, Ashrafi B, Naffakh M, González-Domínguez JM, Johnston A, Simard B *et al.*, *Carbon* **49**:2817–2833 (2011).
4 Gupta S and Tai N, *Carbon* **152**:159–187 (2019).
5 Yadav R, Tirumali M, Wang X, Naebe M and Kandasubramanian B, *Def Technol* **16**:107–118 (2020).
6 Arjmand M, Mahmoodi M, Gelves GA, Park S and Sundararaj U, *Carbon* **49**:3430–3440 (2011).
7 Song L, Xiao M and Meng Y, *Compos Sci Technol* **66**:2156–2162 (2006).
8 Qu S and Wong S, *Compos Sci Technol* **67**:231–237 (2007).
9 Shen W, *Carbon* **37**:351–358 (1999).
10 Yasmin A, Luo J and Daniel IM, *Compos Sci Technol* **66**:1182–1189 (2006).
11 Celzard A, Krzesińska M, Bégin D, Marêché JF, Puricelli S and Furdin G, *Carbon* **40**:557–566 (2002).
12 Liu Y, Zeng J, Han D, Wu K, Yu B, Chai S *et al.*, *Carbon* **133**:435–445 (2018).
13 Zheng W and Wong S, *Compos Sci Technol* **63**:225–235 (2003).
14 Kim H, Hahn HT, Viculis LM, Gilje S and Kaner RB, *Carbon* **45**:1578–1582 (2007).
15 Chen G, Wu D, Weng W, He B and Yan W, *Polym Int* **50**:980–985 (2001).
16 Zheng G, Wu J, Wang W and Pan C, *Carbon* **42**:2839–2847 (2004).
17 Du X, Xiao M, Meng Y and Hay A, *Polymer* **45**:6713–6718 (2004).
18 Weng W, Chen G, Wu D, Chen X, Lu J and Wang P, *J Polym Sci Part B Polym Phys* **42**:2844–2856 (2004).
19 Shen J, Chen X and Huang W, *J Appl Polym Sci* **88**:1864–1869 (2003).

20 Li Y and Chen G, *Polym Eng Sci* **47**:882–888 (2007).
21 Pan Y, Yu Z, Ou Y and Hu G, *J Polym Sci Part B Polym Phys* **38**:1626–1633 (2000).
22 Rinaldi M, Puglia D, Dominici F, Cherubini V, Torre L and Nanni F, *Polym Int* **66**:1731–1736 (2017).
23 Du F, Scogna RC, Zhou W, Brand S, Fischer JE and Winey KI, *Macromolecules* **37**:9048–9055 (2004).
24 Zhang J, Tian W, Chen J, Yu J, Zhang J and Chen J, *Brain Res Bull* **153**: 143–149 (2019).
25 Pei X, Lin L, Schlarb AK and Bennewitz R, *Tribol Int* **136**:462–468 (2019).
26 Schroeder S, Braun S, Mueller U, Vogel M, Sonntag R, Jaeger S *et al*., *J Mech Behav Biomed Mater* **101**:103434 (2020).
27 Flanagan M, Grogan D, Goggins J, Appel S, Doyle K, Leen S *et al*., *Compos A Appl Sci Manuf* **101**:173–184 (2017).
28 Kalra S, Munjal B, Singh VR, Mahajan M and Bhattacharya B, *Adv. Space Res.* **63**:4039–4045 (2019).
29 Shang Y, Liu Y, Wang Z, Jiang Z, Jiang Z and Zhang H, *Polym Int* **66**: 1897–1905 (2017).
30 Xu Q, Shang Y, Jiang Z, Wang Z, Zhou C, Liu X *et al*., *Polym Int* (2020). https://doi.org/10.1002/pi.6166.
31 Li S, Li W, Nie J, Liu D and Sui G, *Carbon* **143**:154–161 (2019).
32 Bessaguet C, Dantras E, Michon G, Chevalier M, Laffont L and Lacabanne C, *J Non-Cryst Solids* **512**:1–6 (2019).
33 Gonçalves J, Lima P, Krause B, Pötschke P, Lafont U, Gomes J *et al*., *Polymers* **10**:925 (2018).
34 Goyal R, *Mater Chem Phys* **142**:195–198 (2013).
35 Mohiuddin M and Hoa S, *Compos Sci Technol* **72**:21–27 (2011).
36 Yang L, Zhang S, Chen Z, Guo Y, Luan J, Geng Z *et al*., *J Mater Sci* **49**: 2372–2382 (2014).
37 Díez-Pascual AM, Naffakh M, González-Domínguez JM, Ansón A, Martínez-Rubi Y, Martinez MT *et al*., *Carbon* **48**:3500–3511 (2010).
38 Diez-Pascual AM, Naffakh M, Gómez M, Marco C, Ellis G, Gonzalez-Dominguez J *et al*., *Nanotechnology* **20**:315707 (2009).
39 Bangarusampath D, Ruckdäschel H, Altstädt V, Sandler JK, Garray D and Shaffer MS, *Polymer* **50**:5803–5811 (2009).
40 Gao C, Han B, Zhang S, Pang J, Wang G and Jiang Z, *Polym Int* **64**:828–832 (2015).
41 Pan L, Liu Z, Zhong L, Pang X, Wang F, Zhu Y *et al*., *Compos Sci Technol* **192**:108117 (2020).
42 Chen B, Berretta S, Evans K, Smith K and Ghita O, *Appl Surf Sci* **428**: 1018–1028 (2018).
43 Zhang H, Zheng W, Yan Q, Yang Y, Wang J, Lu Z *et al*., *Polymer* **51**:1191–1196 (2010).
44 Blundell DJ and Osborn BN, *Polymer* **24**:953–958 (1983).
45 Dhakate S, Sharma S, Borah M, Mathur R and Dhami T, *Int. J. Hydrogen Energy* **33**:7146–7152 (2008).
46 Hussain F, Hojjati M, Okamoto M and Gorga RE, *J Compos Mater* **40**: 1511–1575 (2006).
47 Zhao Y, Xiao M, Wang S, Ge X and Meng Y, *Compos Sci Technol* **67**: 2528–2534 (2007).
48 Kim H and Macosko CW, *Polymer* **50**:3797–3809 (2009).
49 Bangarusampath D, Ruckdäschel H, Altstädt V, Sandler JK, Garray D and Shaffer MS, *Chem Phys Lett* **482**:105–109 (2009).
50 Luo J and Daniel IM, *Compos Sci Technol* **63**:1607–1616 (2003).
51 Fornes T and Paul DR, *Polymer* **44**:4993–5013 (2003).
52 Pryamitsyn V and Ganesan V, *Macromolecules* **39**:844–856 (2006).
53 Sarvestani AS, *Eur Polym J* **44**:263–269 (2008).
54 Kropka JM, Putz KW, Pryamitsyn V, Ganesan V and Green PF, *Macromolecules* **40**:5424–5432 (2007).
55 Zhao J, Morgan AB and Harris JD, *Polymer* **46**:8641–8660 (2005).
56 Sodeifian G, Nikooamal HR and Yousefi AA, *J Polym Res* **19**:9897 (2012).
57 Abbasi S, Carreau PJ, Derdouri A and Moan M, *Rheol Acta* **48**:943–959 (2009).
58 Gupta RK, Pasanovic-Zujo V and Bhattacharya S, *J Non-Newton Fluid Mech* **128**:116–125 (2005).
59 Krishnamoorti R and Yurekli K, *Curr Opin Colloid Interface Sci* **6**:464–470 (2001).
60 Cassagnau PH, *Polymer* **49**:2186–2196 (2008).
61 Le Meins J, Moldenaers P and Mewis J, *Ind Eng Chem Res* **41**:6297–6304 (2002).
62 Papageorgiou DG, Liu M, Li Z, Vallés C, Young RJ and Kinloch IA, *Compos Sci Technol* **175**:60–68 (2019).
63 Alvaredo-Atienza A, Fernández-Blázquez JP, Castell P and de Villoria RG, *Heliyon* **6**:e03740 (2020).
64 Zhang G, Schlarb A, Tria S and Elkedim O, *Compos Sci Technol* **68**:3073–3080 (2008).
65 Rong C, Ma G, Zhang S, Song L, Chen Z, Wang G *et al*., *Compos Sci Technol* **70**:380–386 (2010).
66 Kuo M, Kuo J, Yang M and Huang J, *Mater Chem Phys* **123**:471–480 (2010).
67 Díez-Pascual AM, Naffakh M, Gómez MA, Marco C, Ellis G, Martínez MT *et al*., *Carbon* **47**:3079–3090 (2009).
68 Tewatia A, Hendrix J, Dong Z, Taghon M, Tse S, Chiu G *et al*., *J Mater Sci Eng B* **216**:41–49 (2017).
69 Yu F, Xiao L and Liu Y, *Polym Cryst* **3**:e10103 (2020).
70 Alvaredo Á, Martín MI, Castell P, Guzmán de Villoria R and Fernández-Blázquez JP, *Polymers* **124**:11 (2019).
71 Mariano M, Chirat C, El Kissi N and Dufresne A, *J Polym Sci Part B Polym Phys* **54**:2284–2297 (2016).
72 Fornes T and Paul DR, *Polymer* **44**:3945–3961 (2003).
73 Ramani R and Alam S, *Thermochim Acta* **550**:33–41 (2012).
74 Patel P, Hull TR, McCabe RW, Flath D, Grasmeder J and Percy M, *Polym Degrad Stab* **95**:709–718 (2010).
75 Zhou Z, Zhou F, Zhang S, Mu J, Yue X and Wang G, *Chem Res Chin Univ* **28**:907–911 (2012).
76 Moniruzzaman M and Winey KI, *Macromolecules* **39**:5194–5205 (2006).
77 Zou J, Yu Z, Pan Y, Fang X and Ou Y, *J Polym Sci Part B Polym Phys* **40**: 954–963 (2002).
78 Balberg I, *Phys Rev Lett* **59**:1305–1308 (1987).
79 Debelak B and Lafdi K, *Carbon* **45**:1727–1734 (2007).
80 Sever K, Tavman IH, Seki Y, Turgut A, Omastova M and Ozdemir I, *Compos B Eng* **53**:226–233 (2013).
81 Chung D, *J Mater Sci* **22**:4190–4198 (1987).
82 Kaushik A, Singh P and Bhagat S, *Polym Plast Technol Eng* **48**:802–807 (2009).

